Phosphoproteomic Analysis of Rhodopseudomonas palustris Reveals the Role of Pyruvate Phosphate Dikinase Phosphorylation in Lipid Production

ARTICLE *in* JOURNAL OF PROTEOME RESEARCH · OCTOBER 2012

Impact Factor: 4.25 · DOI: 10.1021/pr300582p · Source: PubMed

Journal of proteome research

Article

pubs.acs.org/jpr

Phosphoproteomic Analysis of *Rhodopseudomonas palustris* Reveals the Role of Pyruvate Phosphate Dikinase Phosphorylation in Lipid Production

Chia-Wei Hu,[†,▽] Miao-Hsia Lin,[‡,▽] Hsuan-Cheng Huang,[§] Wei-Chi Ku,[⊥] Tsun-Hsuan Yi,[†] Chia-Feng Tsai,[∥] Yu-Ju Chen,[∥] Naoyuki Sugiyama,[¶] Yasushi Ishihama,*[,⊥,¶] Hsueh-Fen Juan,*[,†,#] and Shih-Hsiung Wu*[,‡]

[†]Institute of Molecular and Cellular Biology, National Taiwan University, Taipei 106, Taiwan

[‡]Institute of Biological Chemistry, Academia Sinica, Taipei 106, Taiwan

[§]Institute of Biomedical Informatics and Center for Systems and Synthetic Biology, National Yang-Ming University, Taipei 112, Taiwan

[⊥]Graduate School of Pharmaceutical Sciences, Kyoto University, Kyoto 606-8501, Japan

[∥]Institute of Chemistry, Academia Sinica, Taipei 106, Taiwan

[¶]Institute for Advanced Biosciences, Keio University, Tsuruoka 997-0017, Japan

[#]Department of Life Sciences, National Taiwan University, Taipei 106, Taiwan

Supporting Information

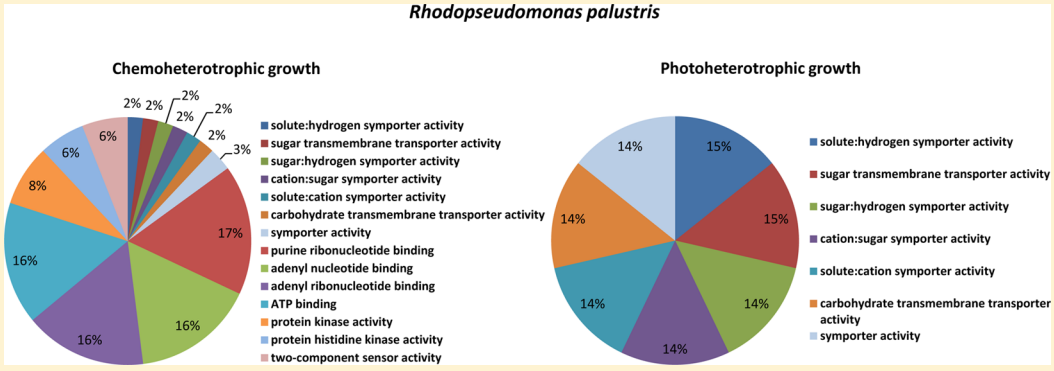

ABSTRACT: *Rhodopseudomonas palustris* (*R. palustris*) is a purple nonsulfur anoxygenic phototrophic bacterium with metabolic versatility and is able to grow under photoheterotrophic and chemoheterotrophic states. It has uses in carbon management, carbon recycling, hydrogen generation, and lipid production; therefore, it has the potential for bioenergy production and biodegradation. This study is the first to identify the phosphoproteome of *R. palustris* including 100 phosphopeptides from 54 phosphoproteins and 74 phosphopeptides from 42 phosphoproteins in chemoheterotrophic and photoheterotrophic growth conditions, respectively. In the identified phosphoproteome, phosphorylation at the threonine residue, Thr487, of pyruvate phosphate dikinase (PPDK, RPA1051) was found to participate in the regulation of carbon metabolism. Here, we show that PPDK enzyme activity is higher in photoheterotrophic growth, with Thr487 phosphorylation as a possible mediator. Under the same photoheterotrophic conditions, *R. palustris* with overexpressed wild-type PPDK showed an enhanced accumulation of total lipids than those with mutant PPDK (T487V) form. This study reveals the role of the PPDK in the production of biodiesel material, lipid content, with threonyl-phosphorylation as one of the possible regulatory events during photoheterotrophic growth in *R. palustris*.

KEYWORDS: *phosphoproteome, photoheterotrophic, pyruvate phosphate dikinase, Rhodopseudomonas palustris, lipid production*

INTRODUCTION

Rhodopseudomonas palustris (*R. palustris*) is a purple nonsulfur anoxygenic photosynthetic bacterium that belongs to alpha-proteobacteria. It is exceptional in its metabolic versatility that it exhibits the ability to grow under photoheterotrophic, photoautotrophic, chemoheterotrophic, and chemoautotrophic conditions, as well as metabolic switch between these four different modes for survival.[1,2] Importantly, *R. palustris* has been selected by the DOE Carbon Management Program for

Received: June 28, 2012
Published: October 2, 2012

   dx.doi.org/10.1021/pr300582p | *J. Proteome Res.* 2012, 11, 5362–5375

genome sequencing because of its ability in carbon management, carbon recycling, hydrogen generation, and lipid production.[1,3−5] Both H_2 and lipids are useful resources for potential alternative candidates for petroleum because they are renewable and less harmful to the environment.[6−8]

There is a growing interest in using bioenergy as a practical approach to obtain environmental, sustainable, and unlimited sources of energy because fossil fuels are exhaustible.[9] Biofuels such as lipids and hydrogen derived from plant oils, animal fats, and microorganisms are now an attractive substitute for petroleum diesel.[7,10,11] Some photosynthetic microorganisms have been reported to offer many industrial benefits and are estimated to produce roughly 100-fold higher yield of lipids per hectare compared to high-lipid plants such as soybeans and sunflowers.[11,12] Therefore, it would be highly beneficial to identify the underlying mechanisms affecting fatty acid production and lipid composition in biofuel production in photosynthetic microorganisms.[6,13] *R. palustris* can convert the energy from sunlight or from a carbon source (e.g., CO_2) to biomass, leading to the storage of carbohydrates and lipids.[1] However, little is known about the regulatory mechanisms of lipids production under different growth conditions in *R. palustris*. Therefore, it is worth conducting further investigations on the physiological regulation of lipid production in these multifunctional bacteria for improved industrial applications, especially in energy production.

Protein phosphorylation plays a significant role in a wide range of physiological processes in both eukaryotic and prokaryotic organisms and is one of the major modes of regulation in signal transduction, growth control, and metabolism. This reversible enzyme-catalyzed process is controlled by various kinases and phosphatases.[14] Phosphorylation of serine/threonine/tyrosine (Ser/Thr/Tyr) residues is considered to be predominant in eukaryotic cells, whereas phosphorylation of histidine/aspartate residues is usually associated with bacterial signaling.[15,16] In general, protein function can be turned on/off by switching between phosphorylated and nonphosphorylated forms in response to environmental changes.[17,18]

To date, a growing body of evidence has demonstrated that Ser/Thr/Tyr protein phosphorylation also contributes to the regulation of a diverse range of cellular responses and physiological processes in prokaryotes.[17,19−21] Recent advances in mass spectrometric techniques combined with genomic sequencing have allowed identification of the scarcely detectable site-specific phosphorylations in bacterial systems.[19] Currently, the phosphoproteomes of several bacterial species including *Bacillus subtilis*, *Escherichia coli*, *Lactococcus lactis*, and *Halobacterium salinarum* as well as some pathogenic bacteria such as *Klebsiella pneumoniae*, *Pseudomonas aeruginosa*, *Salmonella pneumonia*, and *Helicobacter pylori* have been systematically studied.[22−29] These pioneering works have set the foundation of bacterial phosphoproteomics for further addressing of the regulatory events causally relevant to biological issues.

The ability of utilizing various energy sources and substrates depending on different environmental stimuli makes *R. palustris* an ideal model to study the role of phosphorylation in metabolic flexibility and regulation. In this study, the phosphoproteomes from two major metabolic modes (anaerobic photoheterotrophic (PH) and aerobic chemoheterotrophic (CH)) of *R. palustris* were identified to shed light on how their physiological roles can be manipulated by protein phosphorylation. We further found that a phosphoprotein, pyruvate phosphate dikinase (PPDK), which is the key enzyme in carbon metabolism, displayed distinct regulation under different growth conditions and might play a regulatory role in lipid biogenesis in *R. palustris*.

MATERIALS AND METHODS

Cell Culture and Lysate Preparation

R. palustris strain CGA010 was grown under two major metabolic conditions, anaerobic photoheterotrophic (PH) and aerobic chemoheterotrophic (CH). Both cultures were grown in 100 mL bottles at 30 °C to midlog phase ($OD_{660\ nm}$ = 0.6 for CH condition and 0.7 for PH condition). CH cells were grown aerobically in the dark with shaking at 200 rpm; phototrophic cells were grown anaerobically in the light without shaking. All anaerobic cultures were illuminated at a light intensity of 138 $\mu E/m^2/s$. Bacteria grown under both conditions were cultured in photomixotrophic medium (PM).[30] Succinate was added as a carbon source to a final concentration of 10 mM. The cells were collected by centrifugation (25 min at 8000*g*). The cell pellets were resuspended in ice-cold lysis buffer containing 10 mM Tris-HCl (pH 7.4), 1% *N*-octylglucoside (Sigma, St. Louis, MO, USA), protease cocktail (Sigma), and phosphatase inhibitors cocktail (Sigma). Cell walls and cell membranes were broken using an ultrasonic homogenizer (Sartorius, Goettingen, Germany). Cells were exposed to 90% amplitude with a duty cycle of 0.8 s on/0.2 s off. The total sonication time was 2.5 min, and the cellular debris was removed by centrifugation (30 min at 16000*g*).

Protein Digestion

About 2 mg of the protein extract was denatured in 8 M urea (WAKO, Osaka, Japan), reduced with 10 mM DTT (WAKO) at room temperature for 45 min, and carbamidomethylated with 55 mM iodoacetamide (Sigma) at room temperature in darkness for 45 min. Alkylated proteins were digested with endopeptidase Lys-C (1:100 w/w) (WAKO) for 2 h followed by four-time dilution with 50 mM triethylammonium bicarbonate (Sigma). Diluted samples were further digested by sequencing grade modified trypsin (1:100 w/w) (Promega, Mannheim, Germany) overnight at room temperature. The resulting peptide mixture was acidified with TFA to a pH < 3, desalted using StageTips with SDB-XC Empore disk membranes (SDB-XC StageTip) (3M, St. Paul, MN, USA) (31), and eluted in a buffer containing 0.1% TFA and 80% acetonitrile.

Phosphopeptide Enrichment

The phosphopeptides were enriched by hydroxy acid-modified metal oxide chromatography (HAMMOC), as previously described.[27,31,32] The main principle of HAMMOC is to enrich phosphopeptides with the aid of aliphatic hydroxy acid. This approach can reduce the interaction between nonphosphopeptides and the metal oxides, and thus remove most nonphosphopeptides from samples. Briefly, custom-made HAMMOC tips were prepared by packing 0.5-mg TiO_2 beads (10 μm, GL Sciences, Tokyo, Japan) into 10-μL C_8 StageTips. Prior to sample loading, the HAMMOC tips were equilibrated with solution A containing 0.1% TFA, 80% acetonitrile, and 300 mg/mL of lactic acid. About 900 μg of the desalted peptide mixture was mixed with an equal volume of solution A and loaded onto the HAMMOC tips (100 μg of mixed peptides per tip). After successive washing with solution A and solution B (0.1% TFA

dx.doi.org/10.1021/pr300582p | J. Proteome Res. 2012, 11, 5362−5375

and 80% acetonitrile), the resulting phosphopeptides were eluted by 0.5 and 5% piperidine (WAKO). The eluent was acidified with TFA and desalted with SDB-XC StageTip. The desalted phosphopeptides from nine HAMMOC tips were pooled and subjected to further phosphopeptide enrichment using three new HAMMOC tips. This procedure was repeated until phosphopeptides were eluted from only one HAMMOC tip. After desalting with SDB-XC StageTip, the phosphopeptides were resuspended in 0.5% TFA and subjected to nanoliquid chromatography (nanoLC)−MS/MS analysis. For each metabolic condition, two independent batches of samples were prepared.

NanoLC−MS/MS Analysis

Two MS systems, LTQ-Orbitrap XL hybrid mass spectrometer (Thermo Fisher Scientific, Breman, Germany) or TripleTOF 5600 system (AB Sciex, Concord, Canada), were used in this study. Each MS system was coupled with a Dionex Ultimate3000 LC system (Thermo Fisher Scientific) with an HTC-PAL autosampler (CTC Analytics, Zwingen, Switzerland). Peptide mixtures were loaded onto a 100 μm × 150 mm fused-silica capillary column packed with C18 material (3 μm, Dr. Maisch GmbH, Amerbuch Germany). The injection volume for peptide samples was 5 μL, and the flow rate was 500 nL/min. The mobile phases consisted of (A) 0.5% acetic acid and (B) 0.5% acetic acid and 80% acetonitrile. A three-step linear gradient of 5−10% B in 5 min, 10−40% B in 60 min, 40−100% B in 5 min, and 100% B for 10 min was employed throughout this study. For LTQ-Orbitrap XL, the instrument was operated in the positive ion mode, and data was acquired as follows: a full MS scan (m/z 300−1500) was recorded, and the top 10 precursor ions were selected in the MS scan by the Orbitrap detector for subsequent MS/MS scans by ion trap in the automated gain control mode and the automated gain control values of 5.0×10^5 and 1.0×10^4 were set for full MS and MS/MS, respectively. All the measurements in the LTQ-Orbitrap XL were performed with a lock mass.[33] For TripleTOF 5600, the instrument was operated in the positive ion mode, with an ion-spray voltage of 2.3 kV and an interface heater temperature of 150 °C. Data was acquired from one full MS scan (m/z 300−1500) for 250 ms, followed by high-sensitivity MS/MS scans from the top 10 abundant precursor ions, each with a 100-ms accumulation time. For each sample, duplicate nanoLC−MS/MS analyses were performed.

Data Analysis

The peak list of each raw MS spectrum was generated, as previously described.[34] Peptide identification was performed by Mascot v2.3 (Matrix Science, London, UK) against a composite target−decoy protein sequence database containing 4833 *R. palustris* protein sequences and 36 most commonly observed contaminants (http://compbio.ornl.gov/rpal_proteome/databases).[2] The search criteria used in this study were as follows: trypsin specificity allowing up to 2 missed cleavages; fixed modification of carbamidomethyl (C); and variable modifications of oxidation (M) and phosphorylation (ST), (Y), (D), and (H). For data acquisition from LTQ-Orbitrap XL, the precursor mass tolerance was set at 3 ppm, and the fragment ion tolerance was set at 0.8 Da. For data acquisition from TripleTOF 5600, the precursor mass tolerance was set at 10 ppm, and the fragment ion tolerance was set at 0.1 Da. Data from each nanoLC−MS/MS run was searched individually. Peptides were considered identified if the Mascot score yielded a confidence limit above 99% based on the significance threshold ($p < 0.01$) and if at least three successive *y*- or *b*-ions with an additional two and more *y*-, *b*-, and/or precursor-origin neutral loss ions were observed, based on the error-tolerant peptide sequence tag concept.[35] These criteria gave a false-discovery rate of 1.1% for phosphopeptide identification, as evaluated using the target−decoy strategy.[36,37] For those phosphopeptides identified in more than one run, only the one with the highest score has been reported in Supporting InformationTable S1. All the spectra and the related information were submitted to ProteomeXChange (http://www.proteomeexchange.org/, accession PXD000025) and can be inspected by PRIDE Inspector.[38,39]

The reliability of the phosphorylation sites assignments was assessed by two approaches.[34] The first approach was based on the presence of site-determining ions supporting the phosphorylation sites unambiguously, either *y*- or *b*-ions in the peak lists of the fragment ions.[40] This method was only applied to confirm Mascot phosphorylation site assignment. In the other approach, the probability for each of the possible phosphorylation sites was determined by using the PhosCalc version 1.2 (http://www.ayeaye.tsl.ac.uk/PhosCalc/), which was downloaded and modified for evaluating the phosphorylation sites on histidine (H) and aspartate (D).[41] The probability of phosphorylation at all candidate sites within each phosphopeptide was extracted on the basis of the PTM (post-translational modification) score and grouped into class I (phosphosite probability $p > 0.75$), class II ($0.5 < p \leq 0.75$), and class III ($p \leq 0.5$).[42,43] Only a PTM localization probability of >0.75 (class I) was considered as a confident site assignment. On the basis of the difference between the PTM scores of each individual candidate, the "best guess" for phosphorylation sites within each phosphopeptide was assigned.[44]

Bioinformatics Analysis

For functional annotation, the identified phosphoproteins were categorized into respective molecular function classes according to Gene Ontology terms using Blast2GO.[45,46] To gain information on the over-representation of certain protein classes among the identified phosphoproteins, an enrichment analysis was performed using the Fisher test, with p-value < 0.01 being considered statistically significant.

Construction of Functional Interaction Networks

The gene symbols of the identified phosphoproteins were loaded into the database STRING (http://string-db.org/) for construction of functional interaction networks.[47,48] Input proteins and their interaction partners were all represented in the resulting network. Reported interactions included direct (physical) and indirect interactions based on experimental evidence, coregulated gene expression, and the same genomic context or cocitation in the literature. The interactions were filtered with a minimum STRING score of 0.7, which is the default high confidence level in STRING. To cluster the proteins displayed in the networks into families, a Markov clustering (MCL) algorithm, which is specifically suitable for the extraction of complexes from interaction networks, was applied to launch the clustering.[49−51] The clustering process and network presentation were performed using Cytoscape version 2.8.2, an open source bioinformatics software platform for visualizing and integrating molecular interaction networks and biological pathways.[52]

Cloning and Expression of PPDK in *E. coli*

Chromosomal DNA was isolated from the *R. palustris* strain CGA010. The *ppdk* gene (*RPA1051*) was amplified by PCR, using the primer pairs 5′-AATAGCGGCCGCGTC-GAGCTCGCCAACGAAGG-3′ and 5′-GATTC-CATGGCTTCGGCGCCGAACTTGATC-3′. The amplified 2.7-kb DNA fragment was digested with the restriction enzymes *Nde*I and *Hind*III. The digested fragment was purified on a 10% agarose gel and cloned into the pET30a (+) vector (Novagen, Madison, WI, USA) with a C-terminal His-tag (six consecutive histidine residues: HHHHHH) to generate the plasmid pET-*ppdkHis*. Plasmid DNA was prepared and sequenced at the DNA Sequencing Facility (Genomics BioSci & Tech, Taipei, Taiwan). The resulting plasmid (pET-*ppdkHis*) encodes a PPDK-His protein that is 913 amino acids in length and harbors a C-terminal tag of six histidine residues. The resultant plasmid was transformed into the *E. coli* strain BL-21. The positive clones were examined for the expression of the fusion protein. When cells reached an optical density (OD_{600}) of 0.6, expression was induced by adding 0.7 mM isopropyl β-D-1-thiogalactopyranoside (IPTG) (Sigma) to the cell culture at 30 °C. After 3 h, the cell culture was harvested by centrifugation, and the cell pellet was resuspended and sonicated in buffer A (containing 50 mM NaH_2PO_4 [pH 8.0], 300 mM NaCl, 10 mM imidazole, 1% Triton X-100, 1X EDTA-free protease inhibitor cocktail and 1× phosphatase inhibitor cocktail). Cell lysates were centrifuged at 16000*g* for 30 min at 4 °C, and the clear supernatant was saved for further purification. The His-tagged PPDK constructs were purified using a resin containing nickel ions (Ni^{2+}) that had been immobilized by covalently attached nitrilotriacetic acid (NTA). The purified proteins were eluted with 250 mM imidazole, 150 mM NaCl and 20 mM Tris-HCl (pH 8.0). The fractions eluted from the Ni^{2+}-NTA column were resolved on a 12% SDS-PAGE gel. The fractions that contained abundant pure recombinant proteins were stored at −80 °C until further analyses. The same procedure was also used in the purification of PPDK site-specific mutants.

Site-Directed Mutagenesis

Primers containing the desired mutation, flanked by an unmodified nucleotide sequence, are listed below: ppdk-T487V (5′-CGCGGCGGCATGGTCTCGCACGCCGCG-3′); ppdk-T487D (5′-CGCGGCGGCATGGACTCG-CACGCCGCG-3′); and ppdk-H489N (5′-GGCATGACCTC-GAACGCCGCGGTGGTG-3′). Synthesis of the mutant strand was performed by PCR using the plasmid pET-ppdkHis as template in the presence of *PfuTurbo* DNA polymerase (Merck, Darmstadt, Germany). Suitable cycling parameters were chosen according to the QuikChange site-directed mutagenesis kit (Stratagene, La Jolla, CA, USA). At the end of the PCR, 1 μL of the restriction enzyme *Dpn*I (Merck) was added directly to each amplified product, and the reaction was incubated at 37 °C for 1 h. Finally, 1 μL of the *Dpn*I-treated DNA from each amplification reaction was transformed into the *E. coli* strain DH5-alpha. The plasmid DNA (pET-ppdkHisT487V, pET-ppdkHisT487D, and pET-ppdkHisH489N) was prepared and then sequenced at the DNA Sequencing Facility (Genomics BioSci & Tech.).

Overexpression of Wild-Type and Site-Specific Mutant PPDK in *R. palustris*

Plasmid DNA was purified using the Bioman plasmid purification kit (Bioman, Taipei, Taiwan). Phusion high-fidelity DNA polymerase (Finnzymes, Espoo, Finland) was used for amplifying genomic DNA. All the cloning procedures were performed according to the manufacturer's instructions. For cloning, a sticky-end PCR cloning strategy was applied, as previously described.[53] Two pairs of primers (5′-ACACTCGA-GATGGCCAAGTCCGCTG-3′, 5′-CCGTAGT-TACGCCTGGCTGGGATGCC-3′; 5′-ACGTCTAGAT-TACGCCTGGCTGGCG-3′, 5′-ATGGCCAAG-TCCGCTGCAAAGCC-3′) with appropriate restriction sites were used for PCR amplification of the regions flanking the genes of interest. The gene fragments were inserted into XbaI/XhoI-digested pBBR1MCS-5 with a pucBe promoter, using T4 DNA ligase (RBC Bioscience, Taipei, Taiwan).[54] The constructs were transformed into the conjugative strain S-17 and introduced into *R. palustris*.[55,56] Exoconjugants harboring a chromosomal insertion of the plasmid were selected for chloramphenicol and gentamycin resistance to confirm recombination. All the plasmids generated in this study were confirmed by PCR and sequencing. Protein overexpression in each strain was confirmed by subjecting the samples to 8% SDS-PAGE.

PPDK Activity Assay

For measuring endogenous PPDK activity, 20 and 40 μg of cell lysates from each growth condition were used for enzyme activity assays at 30 °C in the phosphoenolpyruvate (PEP)-forming direction spectrophotometrically, as previously described, with minor modifications.[57] The enzyme activity was assayed in 100 mM Tris-HCl (pH 8.0), 10 mM $MgCl_2$, 10 mM $NaHCO_3$, 1.25 mM pyruvate, 1.25 mM ATP, 5 mM DTT, 2.5 mM KH_2PO_4, 0.2 mM NADH, and 6 mM D-glucose 6-phosphate (G-6-P) (Sigma). The reaction was initiated immediately by the addition of malate dehydrogenase (MDH, 2 units) (Sigma) and phosphoenolpyruvate carboxylase (PEPase, 2 units) (Serva, Heidelberg, Germany). The reaction rate was measured by the decrease in absorbance at 340 nm (oxidation of nicotine adenine dinucleotide [NADH] through the coupling enzyme). For the measurement of recombinant PPDK activity, the purified His-tagged PPDK was treated with alkaline phosphatase, calf intestinal (CIP) (New England BioLabs, Beverly, MA, USA) or only with reaction buffer for 30 min at room temperature. The enzyme activities of both phosphorylated and dephosphorylated recombinant PPDK were further analyzed, as described above.

Total Lipid Extraction

The lyophilized bacterial cells in a mortar were extracted with methanol/chloroform (1:2, v/v) for 24 h. A rotary evaporator was used to remove the solvent completely, and the total amount of lipid residues was determined after the cellular extracts were dried to a constant weight.[6]

RESULTS

Phosphoproteome of *R. palustris* under Different Growth Conditions

To reveal the role of protein phosphorylation within the versatile metabolic states of *R. palustris*, the classical shotgun approach was applied to analyze its phosphoproteome.[14] *R. palustris* was separately cultured to midlog phase under PH or CH conditions, and the total proteins were denatured, alkylated, digested and then subjected to phosphopeptide enrichment using HAMMOC (Supporting Information Figure S1). Three-time enrichment with TiO_2 instead of SCX

dx.doi.org/10.1021/pr300582p | J. Proteome Res. 2012, 11, 5362−5375

Table 1. Summary of Phosphopeptides and Phosphorylation Sites Identified in *R. palustris*[a]

acc. number	protein description	phosphopeptides	CH	PH
RPA4793	QxtA cytochrome bd-quinol oxidase subunit I	AAGITPAPAIApTR	*	*
RPA4793	QxtA cytochrome bd-quinol oxidase subunit I	AAGITPAPAIApTRR	*	*
RPA4793	QxtA cytochrome bd-quinol oxidase subunit I	AAGITPAPAIApTRRFS	*	
RPA4760	unknown protein	AApSFSNAAIVSSDK	*	
RPA4760	unknown protein	AASFpSNAAIVSSDK[b]	*	
RPA4760	unknown protein	AASFSNAAIVSpSDK[b]	*	
RPA4524	sensor histidine kinase	AApSLPVATVAAPR	*	
RPA0082	ubiB ubiquinone biosynthesis protein AarF	AELYpSAEAR	*	
RPA4800	possible transporter	ALSpSGAIR	*	*
RPA1140	groEL1 chaperonin GroEL1, cpn60	AQIEETpSSDYDREK	*	
RPA0772	pentapeptide repeat	ASFVSLEGSAFQDSpSMRRAQVVGAK[b]	*	
RPA2513	efp elongation factor P	ATLEVVDTEPVpTK	*	
RPA0225	sodC putative superoxide dismutase (Cu/Zn)	ATLKNAEGTEIGTATLpTESSKGVTIK		*
RPA4587	conserved unknown protein	CGGDPEPALLETpSR[b]	*	
RPA0429	katG catalase/peroxidase	CPFpSGGSHGHR	*	
RPA0432	pnp polyribonucleotide nucleotidyltransferase	DGLVHIpSQLAAGR	*	
RPA2967	glnA glutamine synthetase I	DLpYDLPKEELK	*	*
RPA2967	glnA glutamine synthetase I	DLYpDLPKEELK	*	
RPA2627	putative carboxylesterase	DNASAIGGDAGNVTIFGQpSGGAAK	*	*
RPA3056	nucleoside-diphosphate-kinase	DQAETFpYAVHK	*	*
RPA3056	nucleoside-diphosphate-kinase	DQAETFYAVpHK	*	
RPA1530	bchG geranylgeranyl bacteriochlorophyll synthase	DVDAINEPNRPIPpSGR		*
RPA2446	putative aminotransferase	EALTELIAVAEpSEGIR		*
RPA1548	puhA H subunit of photosynthetic reaction center complex	EGYPLVADAGSGpTR		*
RPA1548	puhA H subunit of photosynthetic reaction center complex	EGYPLVADAGpSGTR		*
RPA2434	sensor histidine kinase	FApYIVSHDLR	*	
RPA1505	putative porphobilinogen deaminase	FETVGDSDQIpSK[b]	*	
RPA3359	RPA3359 O-antigen polymerase	GAERDEAVGpYR	*	
RPA3001	kdpD two component osmosensitive K+channel and sensor histidine kinase, KdpD	GDALIpSAA	*	*
RPA1051	pyruvate phosphate dikinase	GGMTpSHAAVVAR	*	
RPA1051	pyruvate phosphate dikinase	GGMpTSHAAVVAR	*	*
RPA1051	pyruvate phosphate dikinase	GGMTSpHAAVVAR	*	
RPA1051	pyruvate phosphate dikinase	GGMTpSHAAVVAR[b]	*	*
RPA1051	pyruvate phosphate dikinase	GGMpTSHAAVVAR	*	*
RPA4247	fixL two component low oxygen sensor histidine kinase with PAS domains, fixL	GGVVHEDGApSYLCGIVLDIDQQK	*	
RPA4247	fixL two component low oxygen sensor histidine kinase with PAS domains, fixL	GGVVHEDGASpYLCGIVLDIDQQK[b]	*	
RPA1495	unknown protein	GHpSGHPLILK		*
RPA0940	fructose-bisphosphate aldolase	GILAADESSGpTIK[b]	*	
RPA3190	possible dihydrodipicoline synthase related protein	GLLpSSSAQR		*
RPA1484	pgm2 phosphoglucomutase	GRTDGLADGVVVTPSHNPPEpDGGFK		*
RPA1484	pgm2 phosphoglucomutase	GRTDGLADGVVVTPpSHNPPEDGGFK	*	*
RPA1484	pgm2 phosphoglucomutase	GRTDGLADGVVVpTPSHNPPEDGGFK	*	*
RPA3252	tufA, EF-Tu elongation factor Tu	GpSALAALENSDAK	*	
RPA3252	tufA, EF-Tu elongation factor Tu	GSALAALENpSDAK	*	
RPA1495	unknown protein	GYpSGEPLILK		*
RPA1495	unknown protein	GYpSGTPLILEQK		*
RPA4760	unknown protein	HGSGASLADSpSTRLTGAPR[b]	*	
RPA4760	unknown protein	HGSGASLADSSTRLpTGAPR	*	
RPA4760	unknown protein	HGSGASLADpSSTRLTGAPR	*	
RPA2953	hupA possible DNA-binding protein hu-alpha (NS2)	HLAAALAEEHELpSK[b]		*
RPA3252	tufA, EF-Tu elongation factor Tu	HYAHVDCPGHADpYVK[b]		*
RPA1206	aldehyde dehydrogenase	IAFTGETSpTGR	*	
RPA2457	hypothetical protein	IDDWPpSR		*
RPA2457	hypothetical protein	IDDWPpSRR	*	*
RPA2967	glnA glutamine synthetase I	IDPGPAMDKDLpYDLPKEELK		*
RPA2977	nrd ribonucleotide reductase	IGDRAAGAIKSGGpTpTRR		*
RPA0360	pckA phosphoenolpyruvate carboxykinase	IVLIGGTQpYAGEMK		*
RPA1627	cheA2 multidomain chemotaxis histidine kinase CheA2	KpSGGEGEGAAEGGAAGGVANQSIR	*	*

dx.doi.org/10.1021/pr300582p | J. Proteome Res. 2012, 11, 5362−5375

Table 1. continued

acc. number	protein description	phosphopeptides	CH	PH
RPA2005	ABC transporter, fused ATPase and permease domain	LALIGDDDpSPVRKPEIDDDLATSAAAE	*	
RPA2573	possible membrane protein, permease	MLFKPDAKDpTSGAGPGR		*
RPA1525	pufB light-harvesting complex 1 beta chain	MpSDGSISGLSEAEAK[b]	*	
RPA1627	cheA2 multidomain chemotaxis histidine kinase CheA2	MSNLPVIALSpSLVSPAAIER[b]	*	
RPA3201	formate/nitrate transporter	MSpYLAPSEFVTK[b]	*	
RPA0258	unknown protein	NAITQGLLAVGHGDSSpTAR[b]	*	
RPA0354	PTS system phosphocarrier protein HPr, nitrogen regulation	NGETVGGTpSIMGLMMLAAGIGTTVTVSASGPEAR[b]	*	*
RPA0354	PTS system phosphocarrier protein HPr, nitrogen regulation	NGEpTVGGTSIMGLMMLAAGIGTTVTVSASGPEAR	*	*
RPA0354	PTS system phosphocarrier protein HPr, nitrogen regulation	NGETVGGTSIMGLMMLAAGIGTpTVTVSASGPEAR[b]	*	
RPA0198	possible acetate transporter, stationary-phase antideath (SAD) family	NpYTSPFGR	*	
RPA3807	livM putative permease of ABC transporter	QAIpSSDLVK		*
RPA1536	ppsR2 transcriptional regulator PpsR2; Fis family	QALGPIpSK		*
RPA1205	putative alcohol dehydrogenase	QENCDCVISLGGGpSAHDCAK	*	*
RPA0583	sensor histidine kinase with PAS/PAC and Response regulator receiver domains	QSGGHIELpYSEEGHGTTIR	*	*
RPA3355	putative exopolysaccharide polymerization protein	RLEGYSpYR	*	*
RPA3355	putative exopolysaccharide polymerization protein	RLEGYpSYR	*	*
RPA0188	sucB dihydrolipoamide succinyl transferase	RLSTEpSGVDASTVPGSGK	*	
RPA2164	groEL2 chaperonin GroEL2, cpn60	pSADAAGDGTTTATVLAQAIVR	*	
RPA0094	hypothetical protein	pSAGPVVAAPLS		*
RPA0531	beta-ketothiolase, acetoacetyl-CoA thiolase	pSDDVVIVSAAR[b]	*	
RPA4750	etfB electron transfer flavoprotein beta chain, (ETFSS)	pSDGSGVELANVK	*	
RPA1525	pufB light-harvesting complex 1 beta chain	SDGpSISGLSEAEAK	*	
RPA1525	pufB light-harvesting complex 1 beta chain	pSDGSISGLSEAEAK[b]	*	
RPA1712	putative enoyl-CoA hydratase	SDSDpTASAPVLTIDGPR[b]	*	*
RPA2768	rpsI, S9 ribosomal protein S9	SETMQpSLDQLAALK	*	*
RPA2768	rpsI, S9 ribosomal protein S9	pSETMQSLDQLAALK	*	*
RPA2768	rpsI, S9 ribosomal protein S9	SEpTMQSLDQLAALK		*
RPA2768	rpsI, S9 ribosomal protein S9	SEpTMQSLDQLAALK[b]	*	
RPA1627	cheA2 multidomain chemotaxis histidine kinase CheA2	pSGGEGEGAAEGGAAGGVANQSIR	*	
RPA3929	conserved unknown protein	pSGIVLSNAVR	*	
RPA1148	putative sugar transferase	SHGFSpTFSTAR[b]	*	
RPA3355	putative exopolysaccharide polymerization protein	SHpHYpYYYGAPK		*
RPA3355	putative exopolysaccharide polymerization protein	SHHpYYYYGAPK	*	*
RPA3355	putative exopolysaccharide polymerization protein	SHHpYpYYYGAPK	*	*
RPA3355	putative exopolysaccharide polymerization protein	SHHpYpYYpYGAPK	*	
RPA3355	putative exopolysaccharide polymerization protein	SHHpYYpYYGAPK	*	
RPA3355	putative exopolysaccharide polymerization protein	SHHpYYYpYGAPK	*	*
RPA3355	putative exopolysaccharide polymerization protein	SHHYpYYYGAPK	*	*
RPA3355	putative exopolysaccharide polymerization protein	SHHYpYpYYGAPK	*	*
RPA3355	putative exopolysaccharide polymerization protein	SHHYpYpYpYGAPK	*	
RPA3355	putative exopolysaccharide polymerization protein	SHHYpYYpYGAPK	*	*
RPA3355	putative exopolysaccharide polymerization protein	SHHYYpYYGAPK	*	*
RPA3355	putative exopolysaccharide polymerization protein	SHHYYpYpYGAPK	*	*
RPA3355	putative exopolysaccharide polymerization protein	SHHYYYpYGAPK	*	*
RPA3056	nucleoside-diphosphate-kinase	pSIGENSVHGSDAAETAK	*	*
RPA3056	nucleoside-diphosphate-kinase	SIGENSVHGpSDAAETAK	*	*
RPA3056	nucleoside-diphosphate-kinase	SIGENpSVHGSDAAETAK		*
RPA3119	DUF205	SIGpSGNIGATNVLR		*
RPA3119	DUF205	SIGSGNIGApTNVLR	*	*
RPA0190	sucD succinyl-CoA synthetase alpha-subunit	pSILIDSNTR		*
RPA0051	putative sigma-54 modulation protein	SIpSIGEALR	*	*
RPA2082	cobA putative uroporphyrin III methylase	pSKLIESAPAAGR	*	*
RPA2096	cobQ2 cobyric acid synthase	SLMIQGTpSSDVGK		*
RPA2096	cobQ2 cobyric acid synthase	SLMIQGTSpSDVGK		*
RPA2922	rpsB 30S ribosomal protein S2	pSLPEFSMR	*	
RPA2706	manganese transport protein	SPQMTADPSPAPEQpTTGWR	*	
RPA2706	manganese transport protein	SPQMTADPSPAPEQTpTGWR	*	
RPA0605	ptsP nitrogen regulatory protein PTSI(NTR)	SpSDQLALYR		*
RPA2724	glyA1 glycine hydroxymethyltransferase	SpTANPASAPDSFFSASLEQADPEIAAAIR[b]	*	

dx.doi.org/10.1021/pr300582p | J. Proteome Res. 2012, 11, 5362−5375

Table 1. continued

acc. number	protein description	phosphopeptides	CH	PH
RPA0340	pgm1 phosphoglycerate mutase	SVGLPNGQMGNpSEVGHLNIGAGR	*	*
RPA0340	pgm1 phosphoglycerate mutase	SVGLPNGQMGNpSEVGHLNIGAGR	*	*
RPA3201	formate/nitrate transporter	SpYLAPSEFVTK[b]		*
RPA1484	pgm2 phosphoglucomutase	TDGLADGVVVTPpSHNPPEDGGFK	*	*
RPA1998	hypothetical protein	TEQKPpTGRPDTPFPK	*	*
RPA3053	cspA3 cold shock DNA binding protein	TSAENLKIpS	*	
RPA0429	katG catalase/peroxidase	VDLVFGpSHSQLR	*	
RPA0429	katG catalase/peroxidase	VDLVFGSHpSQLR	*	
RPA0185	dldH dihydrolipoamide dehydrogenase	VEVTGADGKATpSVEAK		*
RPA0563	conserved hypothetical protein	VTEWALPGKPpTAR	*	
RPA4679	possible component of multidrug efflux system	VTGPGGNRpTLK		*
RPA0414	DUF167	pYpSAQGVAVAVR	*	

[a]The asterisk indicates the presence of phosphopeptides identified in chemoheterotrophic. [b]Ambiguous phosphorylation site on the peptide, which was determined by manual confirmation as shown in Supporting Information Table S1.

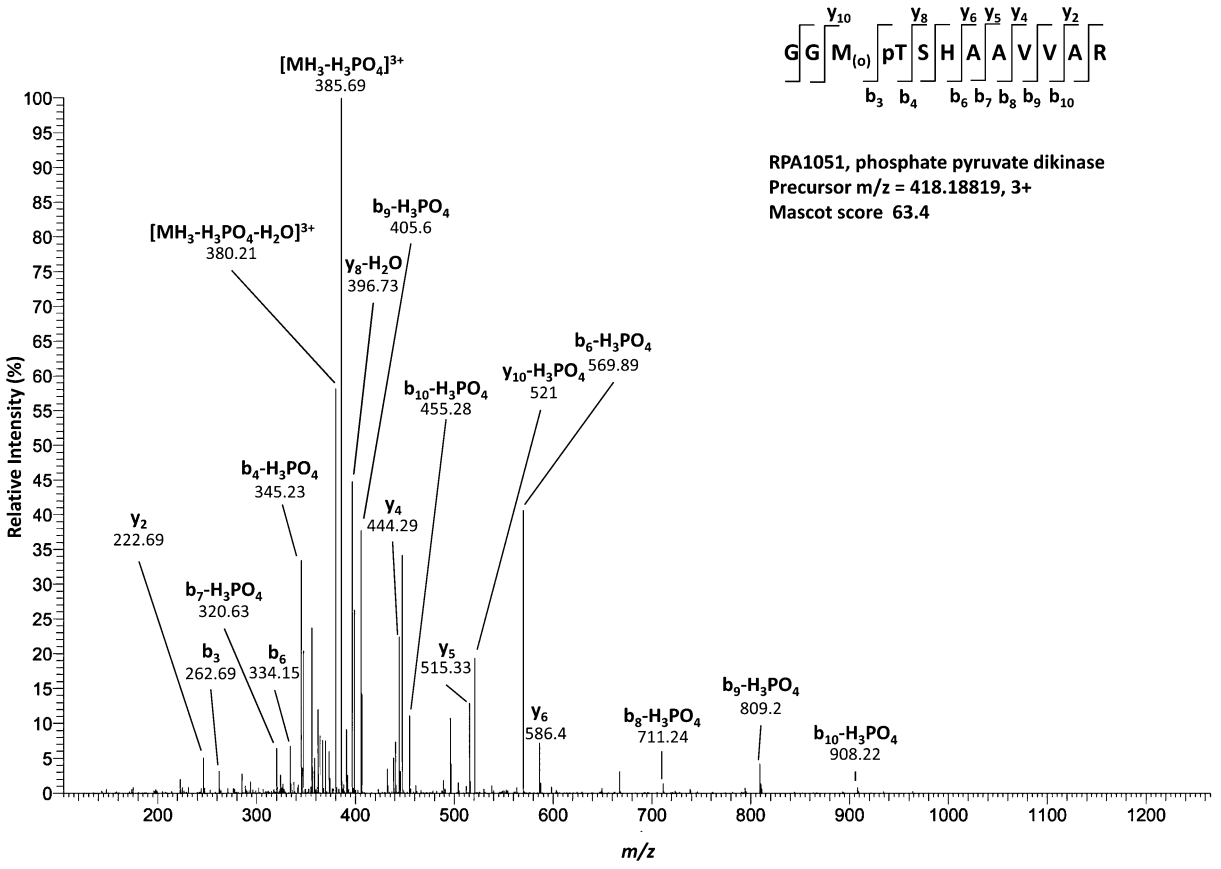

Figure 1. MS/MS spectrum of the phosphopeptide GGMpTSHAAVVAR from pyruvate phosphate dikinase (PPDK). The precursor ion was measured in the LTQ-Orbitrap mass spectrometer. The fragment ions in the MS^2 spectrum localize at the phosphorylation site to Thr^{487}.

fractionation was applied to enhance the identification of phopshopeptides. The captured and eluted peptides from the two preparations were analyzed individually by LC–MS/MS. The resulting MS/MS data were searched against a composite target–decoy protein database, and all confident hits were then compiled into a data set reported in Table 1 and Supporting Information Table S1. Annotated MS/MS spectra of all identified phosphopeptides are presented in Supporting Information Figure S2. An example of a MS/MS spectrum is shown in Figure 1.

We identified a total of 133 unique phosphopeptides with an estimated false-discovery rate of 1.1%, corresponding to 72 phosphoproteins. Among them, 100 unique phosphopeptides were identified from 54 proteins under CH conditions and 74 unique phosphopeptides from 42 proteins under PH conditions, respectively, in *R. palustris* (Table 1). Together, 91 unambiguous Mascot phosphorylation sites were determined from all identified phosphopeptides. 38 serine, 10 threonine, and 12 tyrosine phosphorylation sites were found under CH conditions, yielding a Ser/Thr/Tyr phosphorylation ratio of 63.3/16.1/19.4%. On the other hand, 59 unambiguous Mascot phosphorylation sites containing 33 serines, 13 threonines, and 10 tyrosines were identified under PH

dx.doi.org/10.1021/pr300582p | *J. Proteome Res.* 2012, 11, 5362–5375

conditions that contributed to a Ser/Thr/Tyr phosphorylation ratio of 58.9/23.2/17.9% (Table 2).

Table 2. Number of Identified Phosphopeptides, Phosphoproteins and Phosphorylation Sites from *R. palustris* grown in PH or CH Conditions

variables	chemoheterotrophic	photoheterotrophic
no. of unique phosphopeptides	100	74
no. of identified phosphoproteins	54	42
no. of unique phosphorylation sites (Ser, Thr, Tyr, His, and Asp)	63	59
no. of phosphorylated residues determined by unambiguous Mascot phosphorylated site (Ser:Thr:Tyr)[a]	38:10:12 (63.3:16.1:19.4%)	33:13:10 (58.8:23.2:17.9%)
no. of phosphorylated residues determined by PTM-score derived localization probability (Ser:Thr:Tyr)[b]	21:8:12 (51.2:19.5:29.3%)	20:10:8 (52.6:26.3:21.1%)

[a]The unambiguous phosphorylation site was confirmed based on the presence of site-determining ions supporting the phosphorylation sites as shown in Supporting Information Table S1. [b]Only phosphosites within Class I ($p > 0.75$) in PTM-score derived localization probability results were counted for the proportion of phosphoresidues.

Because the assignment of phosphorylation sites was sometimes uncertain, the probability of phosphorylation localization was calculated using the PTM score, and the "best guess" site for each phosphopeptides was also determined (Supporting Information Tables S1 and S2).[41,44] Among these phosphopeptides, 44 and 41 phosphorylation sites were classified as class I ($p > 0.75$) under CH and PH conditions, respectively (Supporting Information Table S2). A total of 13 and 9 phosphorylation sites were defined as class II ($0.5 < p \leq 0.75$) under CH and PH growth conditions, respectively (Supporting Information Table S2). As shown in Table 2, the phosphorylation ratio of Ser/Thr within class I phosphoresidues was similar with the unambiguous Mascot phosphosities. However, the phosphotyrosine among class I showed a higher proportion as compared with the Mascot results. Besides serine/threonine/tyrosine phosphorylation, protein phosphorylation also includes histidine and aspartate phosphorylation particularly in bacterial system.[58] However, these modifications are difficult to identify since they are unstable in acidic conditions that exist in many experimental steps.[22] In our study, although three histidine and three aspartate residues were also detected as phosphorylated (Class I), none of these findings were supported by the results of "best guess" estimated by the PTM scores. According to the PTM score-derived localization probability, the distribution of serine/threonine in both growth conditions was similar to that observed in other bacterial phosphoproteomes but a higher percentage of tyrosine (Supporting Information Figure S3).[22−24,27]

In our study, only 24 phosphoproteins were identified as being common to both growth conditions (Figure 2A).These coidentified phosphoproteins were mainly involved in carbon metabolism (e.g., RPA1051, pyruvate phosphate dikinase), amino acid synthesis (e.g., RPA2967, glutamine synthetase I), electron transport (e.g., RPA4793, cytochrome bd-quinol oxidase subunit I), and nucleotide metabolism (e.g., RPA3056, nucleoside diphosphate kinase). We further compared the relative abundance of total protein amount according to the previous report on proteomic analysis of *R. palustris*.[2] Among the identified phosphoproteins, most of them showed no significant change in total protein amount. This observation suggests that the changes in phosphoprotein identification might mostly attributable from different regulation on phosphorylation.

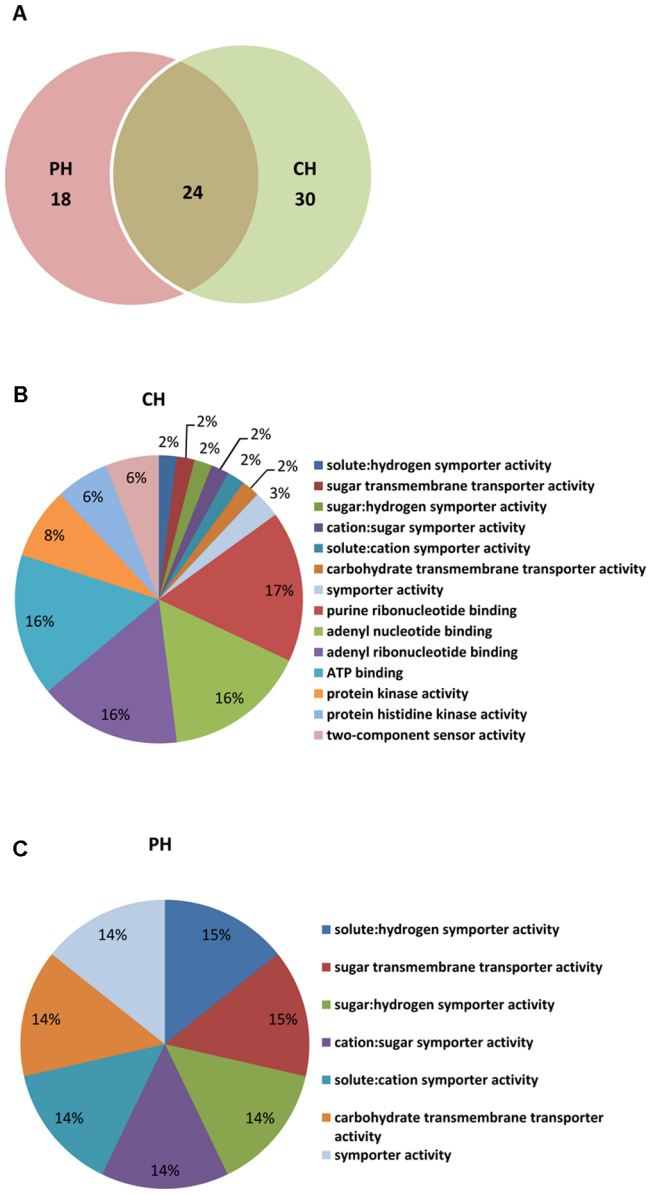

Figure 2. *R. palustris* phosphoproteome. (A) The overlap of phosphoproteins between CH and PH growth. (B) and (C) The molecular functions overrepresented in the phosphoproteins of CH (B) and PH (C). The percentage indicates the number of proteins sharing a certain gene ontology (GO) term relative to the total list of identified phosphoproteins in each condition. CH, chemoheterotrophic condition; PH, photoheterotrophic condition.

Classes of Phosphorylated Proteins in Two Different Growth Conditions

To present an overview of the phosphorylation events in *R. palustris* under CH and PH conditions, the identified phosphoproteins were categorized and enriched according to their molecular functions by Blast2GO, as shown in Figure 2B,C. The characterized phosphoproteins (54 from CH condition and 42 from PH condition) were analyzed against 3670 genes out of the 4833 *R. palustris* genes, which were selected by putative gene ontology annotations as a reference. The analysis showed that the phosphoproteins representative of

dx.doi.org/10.1021/pr300582p | J. Proteome Res. 2012, 11, 5362−5375

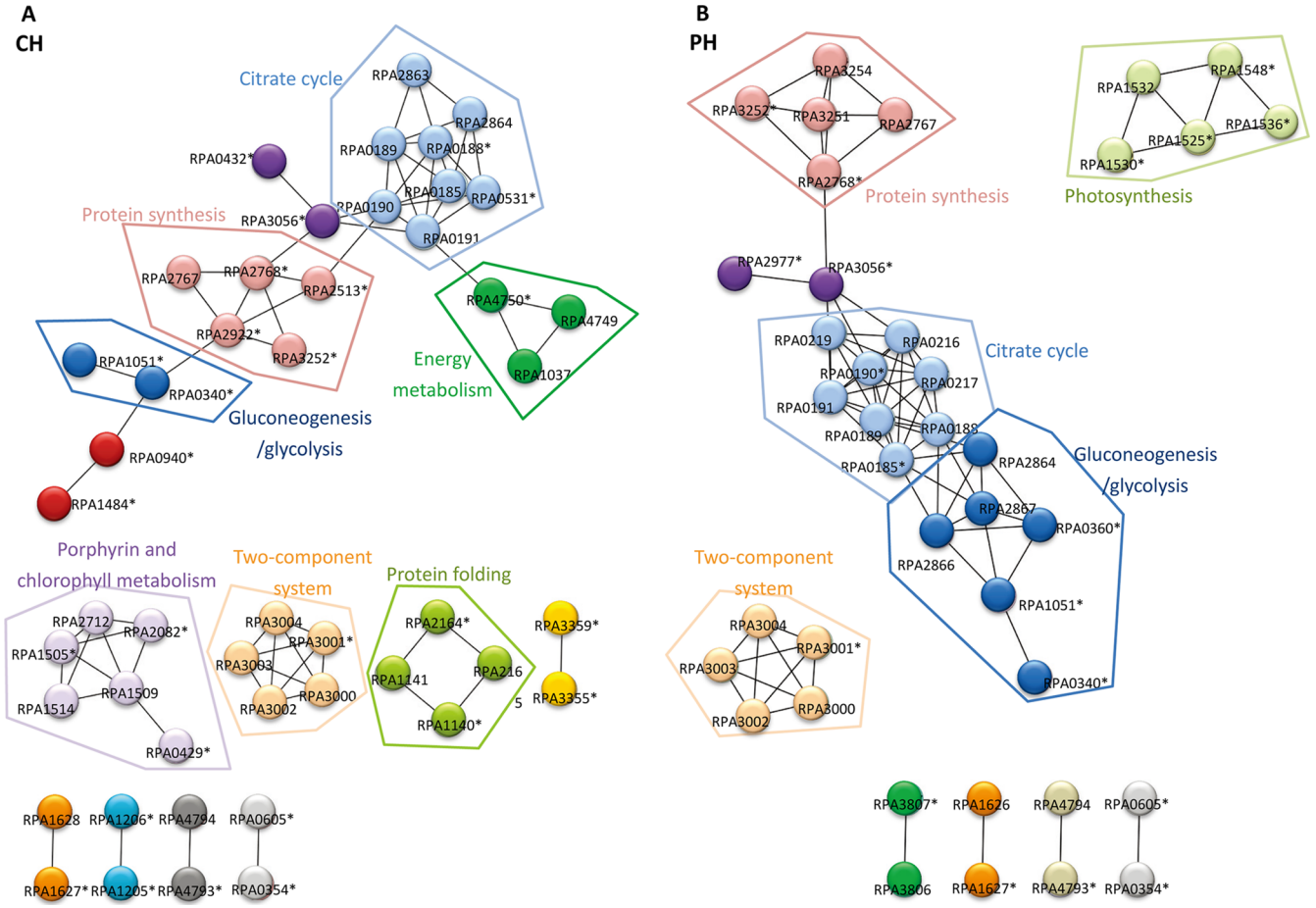

Figure 3. Predicted functional interaction networks of *R. palustris* grown under CH or PH conditions. The predicted interaction networks of phosphoproteins in (A) CH and (B) PH conditions. Both networks were enlarged by additional interacting nodes from STRING. Proteins involved in the same clustering family were represented with the same color. Proteins with asterisks were identified in the phosphoproteomic data.

PH growth were mostly distributed in solute/sugar symporter functions, such as PTS system phosphocarrier protein (RPA0354) and nitrogen regulatory protein PTSI (RPA0605). Most phosphoproteins matched in this category are involved in sugar phosphotransferase system (PTS). On the other side, the phosphoproteins identified under CH growth were overrepresented in ribonucleotide and ATP-binding functions, including katG catalase/peroxidase (RPA0429) and glycine hydroxymethyltransferase (RPA2724).

To further investigate whether phosphorylation regulation was different between the two metabolic states, a functional interaction network analysis was performed. The identified phosphoproteins and their interacting proteins were analyzed and clustered to reveal their functional relationships (Figure 3). Among all the clustering groups, detected proteins were significantly involved in some house-keeping pathways including the citrate cycle, protein synthesis, and gluconeogenesis/glycolysis in both growth conditions.[22,24,26] On the other hand, clusters of protein folding and porphyrin metabolism were enriched in CH condition, whereas photosynthesis was specifically involved in PH condition. The enriched molecular functional and interaction analyses indicate the diverse protein phosphorylation adapted by *R. palustris* as the responses to environmental changes.

Distinct Regulation of Pyruvate Phosphate Dikinase in CH and PH Growth of *R. palustris*

Comparison of the functional interaction networks in two different growth conditions showed that a phosphoprotein, pyruvate phosphate dikinase (RPA1051), was highly connected to other gluconeogenesis/glycolysis proteins, including phosphoenolpyruvate carboxykinase (RPA0360) and phosphoglycerate mutase (RPA0340), in the PH state (Figure 3B), indicating a difference in regulation of PPDK between the two different growth conditions.

In the phosphoproteomic analysis, the phosphorylation site of the identified phosphopeptide, GGMTSHAAVVAR, of PPDK was unambiguously annotated at threonine residue (Thr^{487}) (Figure 1). The relative change of phosphorylated PPDK in the two growth conditions was further analyzed using a label-free approach. Consequently, we found that the amount of Thr^{487}-phosphorylated PPDK peptide was higher in the PH state than in the CH state (Supporting Information Table S3). These results implied that the Thr^{487} phosphorylation of PPDK might play a key role in the regulation of its enzymatic functions in response to environmental variations.

Phosphorylation of Thr^{487} Residue in PPDK Regulates Enzyme Activity

On the basis of the phosphoproteomic and quantitative analysis, the endogenous PPDK activity was speculated to be different under the two growth conditions. Indeed, the PPDK

dx.doi.org/10.1021/pr300582p | *J. Proteome Res.* 2012, 11, 5362−5375

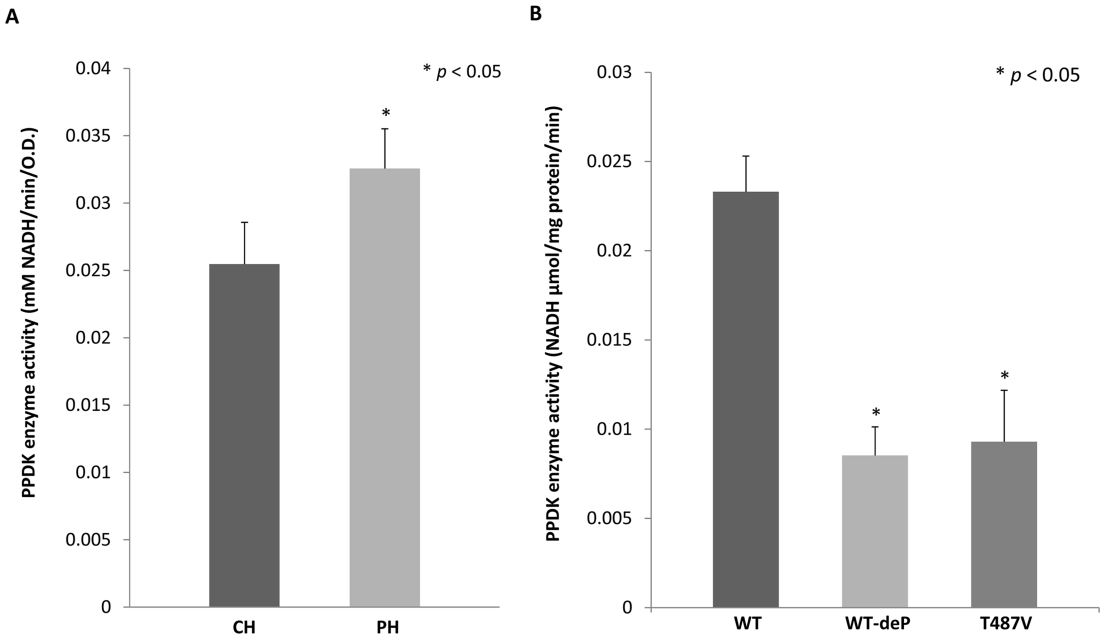

Figure 4. Analysis of PPDK activity. (A) The enzyme activity of endogenous PPDK in *R. palustris* grown under different conditions. CH, chemoheterotrophic condition. PH, photoheterotrophic condition. (B) The enzyme activity of WT PPDK with or without alkaline phosphatase, as well as in the T487V mutant. WT, wild-type PPDK without phosphatase; WT-deP, wild-type PPDK treated with alkaline phosphatase; T487V, mutant PPDK. *P*-value < 0.05 was considered statistically significant.

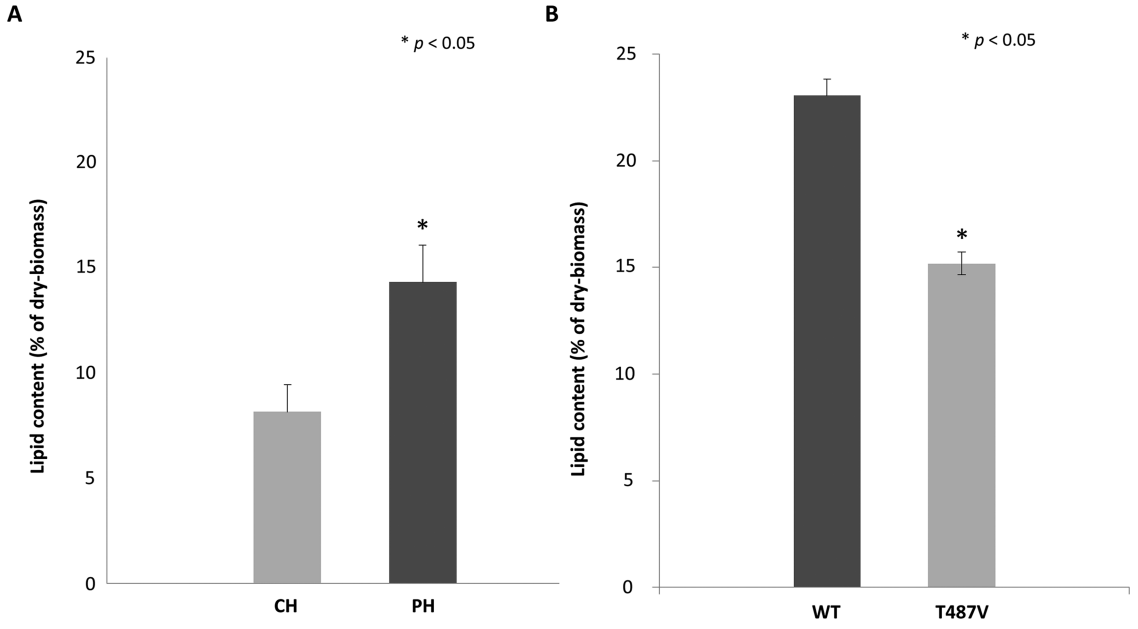

Figure 5. Analysis of total lipid content in *R. palustris.* (A) The total lipid content of *R. palustris* grown under CH or PH conditions. (B) The total lipid content in *R. palustris* showing the overexpression of wild-type PPDK or mutant PPDK. WT, wild-type; T487V, mutant PPDK. Each value represents the mean of triplicate cultures. *P*-value < 0.05 was considered statistically significant.

activity in the PH state was significantly higher with about 1.3-fold increase compared to the CH state (Figure 4A), indicating a light-enhancing effect of the PPDK activity. To elucidate whether PPDK activity was regulated by phosphorylation, the recombinant PPDK proteins that included the wild-type (PPDK) and valine-substituted (PPDKT487V) forms were generated. The phosphorylation states of these recombinant PPDKs were verified by mass spectrometry (Supporting Information Figure S4A and S4B). The similar secondary structures between wild-type and mutant PPDK by circular dichroism spectrometry analysis showed that the mutation does not cause obvious effect on protein folding (Supporting Information Figure S5 and Supporting Information Table S4). The mutant PPDK (T487V) and dephosphorylated forms demonstrated a significant loss of enzymatic activity (Figure 4B). To further confirm the importance of Thr^{487} phosphorylation in PPDK activity, the quantity of nonphosphopeptides in both the phosphorylated and CIP-treated (dephosphorylated) recombinant PPDK forms was estimated by measuring the mass spectral peak area of the peptide "GGMTSHAAVAA"

dx.doi.org/10.1021/pr300582p | *J. Proteome Res.* 2012, 11, 5362−5375

(Supporting Information Table S5). The results revealed a phosphorylation stoichiometry level of 62% with a higher enzyme activity about 4.4-fold in phosphorylated PPDK. These results suggested that a specific regulation of threonyl phosphorylation of PPDK, which is different from the inactivation effect of threonyl phosphorylation of PPDK in C4 plants, exists in *R. palustris*.[59] We hypothesized that this distinction might partially come from the difference in conformational changes resulting from phosphorylation. Therefore, the predicted structures of phosphorylated *R. palustris* and maize PPDKs were generated using homology modeling and molecular dynamics (MD) simulation. Our results revealed a slightly different geometry between the plant and *R. palustris* PPDKs, probably attributable to the differences in conformational changes during Thr phosphorylation (Supporting Information Figure S6). Thus, it is possible to show differential regulation of specific Thr^{487} phosphorylation in PPDKs of plants and prokaryotes.

PPDK Phosphorylation Controlled Total Lipid Biosynthesis

PPDK is a key enzyme involved in glycolysis/gluconeogenesis and CO_2 assimilation, leading to a contribution of biomass synthesis.[60,61] The lipid content in the biomass is believed to be a useful source for biofuel production.[6] To confirm that increased PPDK activity can contribute to biomass synthesis accompanied by higher lipid production, lipid biosynthesis was first compared between the two growth conditions. The results showed that *R. palustris* cultured in the PH state had a larger amount of lipid content than *R. palustris* grown in the CH state (Figure 5A). Furthermore, the wild-type and valine-substituted (T487V) PPDKs were individually overexpressed within *R. palustris* cultured under the PH condition. Both wild-type and mutant (T487V) PPDKs were successfully induced by light, and the wild-type PPDK was demonstrated to be phosphorylated at Thr^{487} (Supporting Information Figure S4C and S4D). Subsequently, as shown in Figure 5B, *R. palustris* containing the wild-type PPDK contained a higher amount of total lipids compared with the mutant PPDK. To further compare lipid composition, the lipid extracts from the wild-type and mutant PPDK- overexpressing cells were analyzed by TLC (Supporting Information Figure S7A). The results showed that the lipid profiles between two bacterial strains were very similar, suggesting no specific type of lipid component were significantly affected by the phosphorylated PPDK. Besides, the growth curve of *R. palustris* with the mutant PPDK (T487V) had a slightly shallower slope, indicating its slower growth (Supporting Information Figure S7B). Therefore, the Thr^{487} phosphorylation of PPDK is likely to play an important role in regulating the physiological metabolism of *R. palustris*, thus affecting its lipid biosynthesis.

DISCUSSION

Recent studies of prokaryotic phosphoproteomes mostly focus on bacterial pathogens with an effort to comprehend how phosphorylation regulates pathogenic functions; however, the systematic understanding of metabolic regulation via protein phosphorylation is still unclear.[62] The metabolically versatile bacterium *R. palustris* is an ideal model organism for bacterial phosphoproteomic studies because its genome has been fully sequenced and annotated. Our study has not only established a global functional distribution of the identified phosphoproteins in *R. palustris*, but also discovered the different phosphorylation patterns in *R. palustris* in different growth conditions. Moreover, on the basis of the previous report on the proteomic study of *R. palustris*, a majority of the identified phosphoproteins showed no obvious change in total protein level between PH and CH conditions.[2] The variation in phosphoprotein profile and the observation in protein level suggested a more important role of protein phosphorylation in *R. palustris* for the adaptation to different environments.

In contrast to plants, the regulation of PPDK in prokaryote is not well-known to date. In the C_4 plants, PPDK activity is strictly regulated via Thr^{487} (Thr^{456} in maize corresponds to Thr^{487} in *R. palustris)* dephosphorylation/phosphorylation in an up/down manner by the level of incident light.[63−65] The PPDK regulatory protein (PDRP), which is a unique bifunctional enzyme, catalyzes this light-dependent regulation by reversible phosphorylation of an active-site Thr residue (Thr^{456} in maize that corresponds to Thr^{487} in *R. palustris*).[63,65] However, unlike the phenomenon in C4 plants, the mutant PPDK (T487V) unable to be phosphorylated resulted in reduced enzyme activity. Besides, the MD simulations of maize and *R. palustris* PPDKs showed that *R. palustris* PPDK might exhibit a small difference in its conformational geometry that originated from Thr^{487} phosphorylation. Although the PPDK sequence is highly conserved among plants and nonplant species, e.g., *R. palustris* and C4 plants shared a 53% similarity in amino acid sequences, the regulatory mechanism appears entirely different between plants and *R. palustris*.[59,66] This is the first study to investigate the importance of Thr phosphorylation in bacterial PPDK and demonstrate that Thr^{487} phosphorylation may play a distinct role in the enzymatic activity from plant.

PPDK can catalyze the ATP- and Pi-dependent formation of PEP, the primary CO_2 acceptor, from pyruvate. This is the rate-limiting step in the C_4 cycle for CO_2 assimilation.[59,66] In addition to its role in CO_2 fixation, PPDK is either a primary or secondary enzyme involved in glycolysis in most nonplant organisms including members of archaea, eubacteria, and protista.[67] Also, PPDK can carry out alternative functions such as gluconeogenesis in the PEP formation direction or glycolytic ATP synthesis in the pyruvate formation direction under anaerobic conditions such as the PH state for *R. palustris*.[60,68−70] Because *R. palustris* can phototropically grow in anaerobic condition, the fine-tuning of PPDK is proposed to be required for CO_2 fixation via glycolysis/gluconeogenesis pathways. Therefore, understanding of the regulatory mechanism in PPDK would extend the knowledge of the metabolic regulation in response to varying environments.

Today, photosynthetic cells such as *R. palustris* have the potential to reduce the elevated atmospheric CO_2 level.[71] The Calvin cycle within photosynthetic cells plays a key role in catalyzing virtually all primary productivity on Earth, making these cells a major sink for atmospheric CO_2.[72] When compared with eukaryotes, bacteria are easier to be genetically manipulated to improve CO_2 assimilation efficiency. Photosynthetic microorganisms like *R. palustris* are by far more efficient than terrestrial plants because of the lower requirements for cultivation space and higher proliferation. Additionally, new photobioreactor designs via the immobilization of photosynthetic organisms create living hybrid materials capable of CO_2 capture and conversion.[73−75] This hybrid material takes living photosynthetic cells and encapsulates them in a biocompatible host structure, thus avoiding competition with food crops. The combination of genetic engineering and advancements in bioreactor designs increases the potential for *R. palustris* to be utilized as a viable large scale carbon sink.

dx.doi.org/10.1021/pr300582p | *J. Proteome Res.* 2012, 11, 5362−5375

In our study, *R. palustris* is suggested to be a model in which PPDK activity can be increased via phosphorylation, thereby leading to higher internal PEP levels and increased rates of lipid biosynthesis. However, this speculation needs to be further investigated using a ^{13}C-labeled substrate. Immobilization of photosynthetic entities within silica scaffolds has been shown to protect cells from harsh environments and even improve their photosynthetic performance.[71,75−77] Accordingly, this successful immobilization approach combined with gene manipulation could be applied in *R. palustris* to improve its growing ability and produce metabolites such as lipid compounds that are capable of being used as biofuels.[71,78,79]

CONCLUSION

In summary, this study revealed the distinct profiles of protein phosphorylation in *R. palustris* from two major metabolic modes, PH and CH. Among them, the phosphorylation level of PPDK was observed to be differentially regulated in PH and CH states. The analysis of enzymatic activity further showed that the phosphorylation on Thr^{487} enhanced the PPDK activity in *R. palustris*. Moreover, comparing to CH growth, the higher phosphorylation level on Thr^{487} of PPDK in PH state affects the production of lipid, which is a kind of biofuel source.

ASSOCIATED CONTENT

Supporting Information

Materials and methods, Tables S1−S5, and Figures S1−S7. This material is available free of charge via the Internet at http://pubs.acs.org.

AUTHOR INFORMATION

Corresponding Author

*(Y.I.) Tel: +81-75-753-4555. Fax: +81-75-753-4601. E-mail: yishiham@pharm.kyoto-u.ac.jp. (H.-F.J.) Tel: +886-2-3366-4536. Fax: +886-2-23673374. E-mail: yukijuan@ntu.edu.tw. (S.-H.W.) Tel: +886-2-2785-5696. Fax: +886-2-26539142. E-mail: shwu@gate.sinica.edu.tw.

Author Contributions

$^{\nabla}$Chia-Wei Hu and Miao-Hsia Lin equally contributed to this work.

Notes

The authors declare no competing financial interest.

ACKNOWLEDGMENTS

We sincerely thank the Core Facilities for Proteomics Research, Academia Sinica, Taiwan, for technical support and Dr. James C. Liao for providing the *R. palustris* strain, CGA010. We also thank Dr. Jiahn-Haur Liao and Dr. Feng-Ling Yang for experimental assistance. This work was supported by the National Science Council of Taiwan (NSC 99-2621-B-002-005-MY3) and the National Taiwan University Cutting-Edge Steering Research Project (10R70602C3).

ABBREVIATIONS

CD, dichroism spectrometry; CH, chemoheterotrophic; DOE, Department of Energy; G-6-P, D-glucose-6-phosphate; HAMMOC, hydroxy acid-modified metal oxide chromatography; IPTG, isopropyl β-D-1-thiogalactopyranoside; MD, molecular dynamics; MDH, malate dehydrogenase; NADH, nicotine adenine dinucleotide; NTA, nitrilotriacetic acid; PEP, phosphoenolpyruvate; PEPase, phosphoenolpyruvate carboxylase; PH, photoheterotrophic; PM, photomixotrophic medium; PPDK, pyruvate phosphate dikinase; PTM, post-translational modification; T487V, valine-substituted mutant PPDK; WT, wild-type PPDK

REFERENCES

(1) Larimer, F. W.; Chain, P.; Hauser, L.; Lamerdin, J.; Malfatti, S.; Do, L.; Land, M. L.; Pelletier, D. A.; Beatty, J. T.; Lang, A. S.; Tabita, F. R.; Gibson, J. L.; Hanson, T. E.; Bobst, C.; Torres, J. L.; Peres, C.; Harrison, F. H.; Gibson, J.; Harwood, C. S. Complete genome sequence of the metabolically versatile photosynthetic bacterium *Rhodopseudomonas palustris*. *Nat. Biotechnol.* **2004**, *22*, 55−61.

(2) VerBerkmoes, N. C.; Shah, M. B.; Lankford, P. K.; Pelletier, D. A.; Strader, M. B.; Tabb, D. L.; McDonald, W. H.; Barton, J. W.; Hurst, G. B.; Hauser, L.; Davison, B. H.; Beatty, J. T.; Harwood, C. S.; Tabita, F. R.; Hettich, R. L.; Larimer, F. W. Determination and comparison of the baseline proteomes of the versatile microbe *Rhodopseudomonas palustris* under its major metabolic states. *J. Proteome Res.* **2006**, *5*, 287−298.

(3) Sasikala, C.; Ramana, C. V. Biodegradation and metabolism of unusual carbon compounds by anoxygenic phototrophic bacteria. *Adv. Microb. Physiol.* **1998**, *39*, 339−377.

(4) Elder, D. J.; Kelly, D. J. The bacterial degradation of benzoic acid and benzenoid compounds under anaerobic conditions: unifying trends and new perspectives. *FEMS Microbiol. Rev.* **1994**, *13*, 441−468.

(5) Barbosa, M. J.; Rocha, J. M.; Tramper, J.; Wijffels, R. H. Acetate as a carbon source for hydrogen production by photosynthetic bacteria. *J. Biotechnol.* **2001**, *85*, 25−33.

(6) Carlozzi, P.; Buccioni, A.; Minieri, S.; Pushparaj, B.; Piccardi, R.; Ena, A.; Pintucci, C. Production of bio-fuels (hydrogen and lipids) through a photofermentation process. *Bioresour. Technol.* **2010**, *101*, 3115−3120.

(7) Carlozzi, P.; Pintucci, C.; Piccardi, R.; Buccioni, A.; Minieri, S.; Lambardi, M. Green energy from *Rhodopseudomonas palustris* grown at low to high irradiance values, under fed-batch operational conditions. *Biotechnol. Lett.* **2010**, *32*, 477−481.

(8) Huang, G.; Chen, F.; Wei, D.; Zhang, X.; Chen, G.. Biodiesel production by microalgal biotechnology. *Appl. Energ.* **2010**, *87*, 38−46.

(9) Hill, J.; Nelson, E.; Tilman, D.; Polasky, S.; Tiffany, D. Environmental, economic, and energetic costs and benefits of biodiesel and ethanol biofuels. *Proc. Natl. Acad. Sci. U. S. A.* **2006**, *103*, 11206−11210.

(10) Rittmann, B. E. Opportunities for renewable bioenergy using microorganisms. *Biotechnol. Bioeng.* **2008**, *100*, 203−212.

(11) Work, V. H.; D'Adamo, S.; Radakovits, R.; Jinkerson, R. E.; Posewitz, M. C. Improving photosynthesis and metabolic networks for the competitive production of phototroph-derived biofuels. *Curr. Opin. Biotechnol.* **2011**, *23*, 290−297.

(12) Rittmann, B. E. Opportunities for renewable bioenergy using microorganisms. *Biotechnol. Bioeng.* **2008**, *100*, 203−212.

(13) Li, Q.; Du, W.; Liu, D. Perspectives of microbial oils for biodiesel production. *Appl. Microbiol. Biotechnol.* **2008**, *80*, 749−756.

(14) Macek, B.; Mann, M.; Olsen, J. V. Global and site-specific quantitative phosphoproteomics: principles and applications. *Annu. Rev. Pharmacol. Toxicol.* **2009**, *49*, 199−221.

(15) Pawson, T.; Scott, J. D. Protein phosphorylation in signaling—50 years and counting. *Trends Biochem. Sci.* **2005**, *30*, 286−290.

(16) Hoch, J. A. Two-component and phosphorelay signal transduction. *Curr. Opin. Microbiol.* **2000**, *3*, 165−170.

(17) Cozzone, A. J. Role of protein phosphorylation on serine/threonine and tyrosine in the virulence of bacterial pathogens. *J. Mol. Microbiol. Biotechnol.* **2005**, *9*, 198−213.

(18) Hess, J. F.; Bourret, R. B.; Simon, M. I. Histidine phosphorylation and phosphoryl group transfer in bacterial chemotaxis. *Nature* **1988**, *336*, 139−143.

(19) Soufi, B.; Jers, C.; Hansen, M. E.; Petranovic, D.; Mijakovic, I. Insights from site-specific phosphoproteomics in bacteria. *Biochim. Biophys. Acta* **2008**, *1784*, 186−192.

(20) Cozzone, A. J.; Grangeasse, C.; Doublet, P.; Duclos, B. Protein phosphorylation on tyrosine in bacteria. *Arch. Microbiol.* **2004**, *181*, 171−181.
(21) Backert, S.; Selbach, M. Tyrosine-phosphorylated bacterial effector proteins: the enemies within. *Trends Microbiol.* **2005**, *13*, 476−484.
(22) Macek, B.; Mijakovic, I.; Olsen, J. V.; Gnad, F.; Kumar, C.; Jensen, P. R.; Mann, M. The serine/threonine/tyrosine phosphoproteome of the model bacterium *Bacillus subtilis*. *Mol. Cell. Proteomics* **2007**, *6*, 697−707.
(23) Macek, B.; Gnad, F.; Soufi, B.; Kumar, C.; Olsen, J. V.; Mijakovic, I.; Mann, M. Phosphoproteome analysis of *E. coli* reveals evolutionary conservation of bacterial Ser/Thr/Tyr phosphorylation. *Mol. Cell. Proteomics* **2008**, *7*, 299−307.
(24) Soufi, B.; Gnad, F.; Jensen, P. R.; Petranovic, D.; Mann, M.; Mijakovic, I.; Macek, B. The Ser/Thr/Tyr phosphoproteome of *Lactococcus lactis* IL1403 reveals multiply phosphorylated proteins. *Proteomics* **2008**, *8*, 3486−3493.
(25) Aivaliotis, M.; Macek, B.; Gnad, F.; Reichelt, P.; Mann, M.; Oesterhelt, D. Ser/Thr/Tyr protein phosphorylation in the archaeon *Halobacterium salinarum*—a representative of the third domain of life. *PLoS One* **2009**, *4*, e4777.
(26) Lin, M. H.; Hsu, T. L.; Lin, S. Y.; Pan, Y. J.; Jan, J. T.; Wang, J. T.; Khoo, K. H.; Wu, S. H. Phosphoproteomics of *Klebsiella pneumoniae* NTUH-K2044 reveals a tight link between tyrosine phosphorylation and virulence. *Mol. Cell. Proteomics* **2009**, *8*, 2613−2623.
(27) Ravichandran, A.; Sugiyama, N.; Tomita, M.; Swarup, S.; Ishihama, Y. Ser/Thr/Tyr phosphoproteome analysis of pathogenic and non-pathogenic Pseudomonas species. *Proteomics* **2009**, *9*, 2764−2775.
(28) Sun, X.; Ge, F.; Xiao, C. L.; Yin, X. F.; Ge, R.; Zhang, L. H.; He, Q. Y. Phosphoproteomic analysis reveals the multiple roles of phosphorylation in pathogenic bacterium *Streptococcus pneumoniae*. *J. Proteome Res.* **2010**, *9*, 275−282.
(29) Ge, R.; Sun, X.; Xiao, C.; Yin, X.; Shan, W.; Chen, Z.; He, Q. Y. Phosphoproteome analysis of the pathogenic bacterium *Helicobacter pylori* reveals over-representation of tyrosine phosphorylation and multiply phosphorylated proteins. *Proteomics* **2011**, *11*, 1449−1461.
(30) Dispensa, M.; Thomas, C. T.; Kim, M. K.; Perrotta, J. A.; Gibson, J.; Harwood, C. S. Anaerobic growth of *Rhodopseudomonas palustris* on 4-hydroxybenzoate is dependent on AadR, a member of the cyclic AMP receptor protein family of transcriptional regulators. *J. Bacteriol.* **1992**, *174*, 5803−5813.
(31) Rappsilber, J.; Mann, M.; Ishihama, Y. Protocol for micro-purification, enrichment, pre-fractionation and storage of peptides for proteomics using StageTips. *Nat. Protoc.* **2007**, *2*, 1896−1906.
(32) Sugiyama, N.; Masuda, T.; Shinoda, K.; Nakamura, A.; Tomita, M.; Ishihama, Y. Phosphopeptide enrichment by aliphatic hydroxy acid-modified metal oxide chromatography for nano-LC−MS/MS in proteomics applications. *Mol. Cell. Proteomics* **2007**, *6*, 1103−1109.
(33) Olsen, J. V.; de Godoy, L. M.; Li, G.; Macek, B.; Mortensen, P.; Pesch, R.; Makarov, A.; Lange, O.; Horning, S.; Mann, M. Parts per million mass accuracy on an Orbitrap mass spectrometer via lock mass injection into a C-trap. *Mol. Cell. Proteomics* **2005**, *4*, 2010−2021.
(34) Nakagami, H.; Sugiyama, N.; Mochida, K.; Daudi, A.; Yoshida, Y.; Toyoda, T.; Tomita, M.; Ishihama, Y.; Shirasu, K. Large-scale comparative phosphoproteomics identifies conserved phosphorylation sites in plants. *Plant Physiol.* **2010**, *153*, 1161−1174.
(35) Mann, M.; Wilm, M. Error-tolerant identification of peptides in sequence databases by peptide sequence tags. *Anal. Chem.* **1994**, *66*, 4390−4399.
(36) Munton, R. P.; Tweedie-Cullen, R.; Livingstone-Zatchej, M.; Weinandy, F.; Waidelich, M.; Longo, D.; Gehrig, P.; Potthast, F.; Rutishauser, D.; Gerrits, B.; Panse, C.; Schlapbach, R.; Mansuy, I. M. Qualitative and quantitative analyses of protein phosphorylation in naive and stimulated mouse synaptosomal preparations. *Mol. Cell. Proteomics* **2007**, *6*, 283−293.
(37) Endler, A.; Reiland, S.; Gerrits, B.; Schmidt, U. G.; Baginsky, S.; Martinoia, E. In vivo phosphorylation sites of barley tonoplast proteins identified by a phosphoproteomic approach. *Proteomics* **2009**, *9*, 310−321.
(38) Vizcaino, J. A.; Cote, R.; Reisinger, F.; Barsnes, H.; Foster, J. M.; Rameseder, J.; Hermjakob, H.; Martens, L. The Proteomics Identifications database: 2010 update. *Nucleic Acids Res.* **2010**, *38*, D736−742.
(39) Wang, R.; Fabregat, A.; Rios, D.; Ovelleiro, D.; Foster, J. M.; Cote, R. G.; Griss, J.; Csordas, A.; Perez-Riverol, Y.; Reisinger, F.; Hermjakob, H.; Martens, L.; Vizcaino, J. A. PRIDE Inspector: a tool to visualize and validate MS proteomics data. *Nat. Biotechnol.* **2012**, *30*, 135−137.
(40) Sugiyama, N.; Nakagami, H.; Mochida, K.; Daudi, A.; Tomita, M.; Shirasu, K.; Ishihama, Y. Large-scale phosphorylation mapping reveals the extent of tyrosine phosphorylation in *Arabidopsis*. *Mol. Syst. Biol.* **2008**, *4*, 193.
(41) MacLean, D.; Burrell, M. A.; Studholme, D. J.; Jones, A. M. PhosCalc: a tool for evaluating the sites of peptide phosphorylation from mass spectrometer data. *BMC Res. Notes* **2008**, *1*, 30.
(42) Olsen, J. V.; Blagoev, B.; Gnad, F.; Macek, B.; Kumar, C.; Mortensen, P.; Mann, M. Global, in vivo, and site-specific phosphorylation dynamics in signaling networks. *Cell* **2006**, *127*, 635−648.
(43) Masuda, T.; Sugiyama, N.; Tomita, M.; Ishihama, Y. Microscale phosphoproteome analysis of 10,000 cells from human cancer cell lines. *Anal. Chem.* **2011**, *83*, 7698−7703.
(44) Kyono, Y.; Sugiyama, N.; Tomita, M.; Ishihama, Y. Chemical dephosphorylation for identification of multiply phosphorylated peptides and phosphorylation site determination. *Rapid Commun. Mass Spectrom.* **2010**, *24*, 2277−2282.
(45) Gotz, S.; Garcia-Gomez, J. M.; Terol, J.; Williams, T. D.; Nagaraj, S. H.; Nueda, M. J.; Robles, M.; Talon, M.; Dopazo, J.; Conesa, A. High-throughput functional annotation and data mining with the Blast2GO suite. *Nucleic Acids Res.* **2008**, *36*, 3420−3435.
(46) Conesa, A.; Gotz, S.; Garcia-Gomez, J. M.; Terol, J.; Talon, M.; Robles, M. Blast2GO: a universal tool for annotation, visualization and analysis in functional genomics research. *Bioinformatics* **2005**, *21*, 3674−3676.
(47) Snel, B.; Lehmann, G.; Bork, P.; Huynen, M. A. STRING: a web-server to retrieve and display the repeatedly occurring neighbourhood of a gene. *Nucleic Acids Res.* **2000**, *28*, 3442−3444.
(48) Szklarczyk, D.; Franceschini, A.; Kuhn, M.; Simonovic, M.; Roth, A.; Minguez, P.; Doerks, T.; Stark, M.; Muller, J.; Bork, P.; Jensen, L. J.; von Mering, C. The STRING database in 2011: functional interaction networks of proteins, globally integrated and scored. *Nucleic Acids Res.* **2011**, *39*, D561−568.
(49) Dongen, S. M. v. Graph clustering by flow simulation. Ph.D. Thesis, University of Utrecht, The Netherlands, 2000.
(50) Enright, A. J.; Van Dongen, S.; Ouzounis, C. A. An efficient algorithm for large-scale detection of protein families. *Nucleic Acids Res.* **2002**, *30*, 1575−1584.
(51) Brohee, S.; van Helden, J. Evaluation of clustering algorithms for protein-protein interaction networks. *BMC Bioinf.* **2006**, *7*, 488.
(52) Shannon, P.; Markiel, A.; Ozier, O.; Baliga, N. S.; Wang, J. T.; Ramage, D.; Amin, N.; Schwikowski, B.; Ideker, T. Cytoscape: a software environment for integrated models of biomolecular interaction networks. *Genome Res.* **2003**, *13*, 2498−2504.
(53) Shih, Y. P.; Kung, W. M.; Chen, J. C.; Yeh, C. H.; Wang, A. H.; Wang, T. F. High-throughput screening of soluble recombinant proteins. *Protein Sci.* **2002**, *11*, 1714−1719.
(54) Kovach, M. E.; Elzer, P. H.; Hill, D. S.; Robertson, G. T.; Farris, M. A.; Roop, R. M., 2nd; Peterson, K. M. Four new derivatives of the broad-host-range cloning vector pBBR1MCS, carrying different antibiotic-resistance cassettes. *Gene* **1995**, *166*, 175−176.
(55) Simon, R.; Priefer, U.; Puhler, A. A Broad Host range mobilization system for in vivo genetic engineering: transposon mutagenesis in gram negative Bacteria. *Nat. Biotechnol.* **1983**, *1*, 784−791.

(56) Romagnoli, S.; Tabita, F. R. A novel three-protein two-component system provides a regulatory twist on an established circuit to modulate expression of the cbbI region of *Rhodopseudomonas palustris* CGA010. *J. Bacteriol.* **2006**, *188*, 2780−2791.
(57) Salahas, G.; Manetas, Y.; Gavalas, N. A. Assaying for pyruvate, orthophosphate dikinase activity: Necessary precautions with phosphoenolpyruvate carboxylase as coupling enzyme. *Photosynth. Res.* **1990**, *24*, 183−188.
(58) Dutta, R.; Qin, L.; Inouye, M. Histidine kinases: diversity of domain organization. *Mol. Microbiol.* **1999**, *34*, 633−640.
(59) Pocalyko, D. J.; Carroll, L. J.; Martin, B. M.; Babbitt, P. C.; Dunaway-Mariano, D. Analysis of sequence homologies in plant and bacterial pyruvate phosphate dikinase, enzyme I of the bacterial phosphoenolpyruvate: sugar phosphotransferase system and other PEP-utilizing enzymes. Identification of potential catalytic and regulatory motifs. *Biochemistry* **1990**, *29*, 10757−10765.
(60) Chastain, C. J.; Botschner, M.; Harrington, G. E.; Thompson, B. J.; Mills, S. E.; Sarath, G.; Chollet, R. Further analysis of maize C(4) pyruvate,orthophosphate dikinase phosphorylation by its bifunctional regulatory protein using selective substitutions of the regulatory Thr-456 and catalytic His-458 residues. *Arch. Biochem. Biophys.* **2000**, *375*, 165−170.
(61) Reeves, R. E. A new enzyme with the glycolytic function of pyruvate kinase. *J. Biol. Chem.* **1968**, *243*, 3202−3204.
(62) Jers, C.; Soufi, B.; Grangeasse, C.; Deutscher, J.; Mijakovic, I. Phosphoproteomics in bacteria: towards a systemic understanding of bacterial phosphorylation networks. *Expert Rev. Proteomics* **2008**, *5*, 619−627.
(63) Budde, R. J.; Holbrook, G. P.; Chollet, R. Studies on the dark/light regulation of maize leaf pyruvate, orthophosphate dikinase by reversible phosphorylation. *Arch. Biochem. Biophys.* **1985**, *242*, 283−290.
(64) Burnell, J. N.; Hatch, M. D. Regulation of C4 photosynthesis: purification and properties of the protein catalyzing ADP-mediated inactivation and Pi-mediated activation of pyruvate,Pi dikinase. *Arch. Biochem. Biophys.* **1985**, *237*, 490−503.
(65) Burnell, J. N.; Hatch, M. D. Dark-light regulation of pyruvate, Pi dikinase in C4 plants: evidence that the same protein catalyses activation and inactivation. *Biochem. Biophys. Res. Commun.* **1983**, *111*, 288−293.
(66) Hatch, M. D.; Slack, C. R. Studies on the mechanism of activation and inactivation of pyruvate, phosphate dikinase. A possible regulatory role for the enzyme in the C4 dicarboxylic acid pathway of photosynthesis. *Biochem. J.* **1969**, *112*, 549−558.
(67) Fisslthaler, B.; Meyer, G.; Bohnert, H. J.; Schmitt, J. M. Age-dependent induction of pyruvate, orthophosphate dikinase in *Mesembryanthemum crystallinum* L. *Planta* **1995**, *196*, 492−500.
(68) Roeske, C. A.; Chollet, R. Chemical modification of the bifunctional regulatory protein of maize leaf pyruvate,orthophosphate dikinase. Evidence for two distinct active sites. *J. Biol. Chem.* **1987**, *262*, 12575−12582.
(69) Matsuoka, M. The gene for pyruvate, orthophosphate dikinase in C4 plants: structure, regulation and evolution. *Plant Cell Physiol.* **1995**, *36*, 937−943.
(70) Chastain, C. J.; Failing, C. J.; Manandhar, L.; Zimmerman, M. A.; Lakner, M. M.; Nguyen, T. H. T. Functional evolution of C4 pyruvate, orthophosphate dikinase. *J. Exp. Bot.* **2011**, *62*, 3083−3091.
(71) Su, B. L.; Meunier, C. F.; Rooke, J. C.; Leonard, A.; Xie, H. Living hybrid materials capable of energy conversion and CO_2 assimilation. *Chem. Commun.* **2010**, *46*, 3843−3859.
(72) McKinlay, J. B.; Harwood, C. S. Carbon dioxide fixation as a central redox cofactor recycling mechanism in bacteria. *Proc. Natl. Acad. Sci. U. S. A.* **2010**, *107*, 11669−11675.
(73) Rooke, J. C.; Leonard, A.; Sarmento, H.; Descy, J.-P.; Su, B.-L. Photosynthesis within porous silica gel: viability and activity of encapsulated cyanobacteria. *J. Mater. Chem.* **2008**, *18*, 2833−2841.
(74) Ugwu, C. U.; Aoyagi, H.; Uchiyama, H. Photobioreactors for mass cultivation of algae. *Bioresour. Technol.* **2008**, *99*, 4021−4028.
(75) Rooke, J. C.; Leonard, A.; Sarmento, H.; Meunier, C. F.; Descy, J.-P.; Su, B.-L. Novel photosynthetic CO_2 bioconvertor based on green algae entrapped in low-sodium silica gels. *J. Mater. Chem.* **2011**, *21*, 951−959.
(76) Meunier, C. F.; Cutsem, P. V.; Kwon, Y.-U.; Su, B.-L. Investigation of different silica precursors: Design of biocompatible silica gels with long term bio-activity of entrapped thylakoids toward artificial leaf. *J. Mater. Chem.* **2009**, *19*, 4131−4137.
(77) Meunier, C. F.; Van Cutsem, P.; Kwon, Y.-U.; Su, B.-L. Thylakoids entrapped within porous silica gel: towards living matter able to convert energy. *J. Mater. Chem.* **2009**, *19*, 1535−1542.
(78) Ratledge, C.; Wynn, J. P. The biochemistry and molecular biology of lipid accumulation in oleaginous microorganisms. *Adv. Appl. Microbiol.* **2002**, *51*, 1−51.
(79) Chisti, Y. Biodiesel from microalgae. *Biotechnol. Adv.* **2007**, *25*, 294−306.